MCB
Journals.ASM.org

Sonic hedgehog-Dependent Induction of MicroRNA 31 and MicroRNA 150 Regulates *Mycobacterium bovis* BCG-Driven Toll-Like Receptor 2 Signaling

Devram Sampat Ghorpade,[a] Sahana Holla,[a] Srini V. Kaveri,[b,c] Jagadeesh Bayry,[b,c] Shripad A. Patil,[d] Kithiganahalli Narayanaswamy Balaji[a]

Department of Microbiology and Cell Biology, Indian Institute of Science, Bangalore, India[a]; Institut National de la Santé et de la Recherche Médicale, Unité 872, Equipe 16-Immunopathology and Therapeutic Immunointervention, Paris, France[b]; Unité Mixte de Recherche S 872, Centre de Recherche des Cordeliers, Equipe 16-Immunopathology and Therapeutic Immunointervention, Université Pierre et Marie Curie-Paris 6, Paris, France[c]; Department of Microbiology, National Institute of Mental Health and Neurosciences, Bangalore, India[d]

Hedgehog (HH) signaling is a significant regulator of cell fate decisions during embryogenesis, development, and perpetuation of various disease conditions. Testing whether pathogen-specific HH signaling promotes unique innate recognition of intracellular bacteria, we demonstrate that among diverse Gram-positive or Gram-negative microbes, *Mycobacterium bovis* BCG, a vaccine strain, elicits a robust activation of Sonic HH (SHH) signaling in macrophages. Interestingly, sustained tumor necrosis factor alpha (TNF-α) secretion by macrophages was essential for robust SHH activation, as TNF-$\alpha^{-/-}$ macrophages exhibited compromised ability to activate SHH signaling. Neutralization of TNF-α or blockade of TNF-α receptor signaling significantly reduced the infection-induced SHH signaling activation both *in vitro* and *in vivo*. Intriguingly, activated SHH signaling downregulated *M. bovis* BCG-mediated Toll-like receptor 2 (TLR2) signaling events to regulate a battery of genes associated with divergent functions of M1/M2 macrophages. Genome-wide expression profiling as well as conventional gain-of-function or loss-of-function analysis showed that SHH signaling-responsive microRNA 31 (miR-31) and miR-150 target MyD88, an adaptor protein of TLR2 signaling, thus leading to suppression of TLR2 responses. SHH signaling signatures could be detected *in vivo* in tuberculosis patients and *M. bovis* BCG-challenged mice. Collectively, these investigations identify SHH signaling to be what we believe is one of the significant regulators of host-pathogen interactions.

During the ensuing immunity to invading pathogens, numerous signaling molecules are repurposed to execute specific functions in divergent cellular contexts. Sonic hedgehog (SHH), a pleotropic member of the hedgehog family of signaling molecules, plays key roles in vascular embryonic development (1, 2), wound healing (3), as well as development of various tissues and organs, including brain, heart, and thymus (4, 5). Despite a comprehensive understanding of the signaling events participating downstream of SHH, relatively little is known in regard to the nature of genes that mediate cell fate specifications by SHH in immune cells like macrophages. Significantly, recognition and amplification of pathogen-specific signaling events play important roles not only in discriminating the invading microbes but also in regulating explicit immune responses (6–13). In this context, integration of key signaling centers modulating immunity to pathogenic mycobacterial infections remains unexplored. However, macrophages as sentinels are known to tailor differential immune responses to infections with pathogenic mycobacteria, including *Mycobacterium tuberculosis*, *Mycobacterium bovis*, etc., by utilizing dynamic interplay of signaling networks (14–19). We propose SHH signaling to constitute one such signaling network.

Canonical SHH signaling that mediates cell fate decisions requires binding of SHH to its cognate receptor, Patched (PTCH1), resulting in alleviating the inhibition of a seven-pass transmembrane protein, Smoothened (SMO). The resultant conformational changes in SMO lead to the activation of the GLI family of transcription factors, which often act as rate-limiting elements in defining cell fate specifications (20). In the off state, GLI3, a well-known inhibitor of the SHH pathway, is subjected to modifications through a cytosolic inhibitory complex comprising glycogen synthase kinase 3β (GSK-3β), which makes GLI3 a transcriptional repressor (21, 22). However, SMO activation subdues the inhibitory complex, thereby rendering GLI3 inactive and inducing the transactivatory GLI1 functions (23). Interestingly, NUMB-induced GLI1 ubiquitination contributes to the tight regulation of the SHH pathway to determine cell fate decisions (24).

In view of the observations described above, we set out to unravel the molecular mechanisms contributing toward pathogen-specific activation of SHH signaling in macrophages. The present investigation demonstrates that *M. bovis* BCG, a vaccine strain, triggers a robust activation of SHH signaling in macrophages compared to infection with diverse Gram-positive or Gram-negative microbes. This observation was further evidenced in the *in vivo* scenario with pulmonary tuberculosis (TB) individuals as well as tuberculous meningitis (TBM) patients exhibiting heightened SHH signaling. Furthermore, experiments utilizing anti-tu-

Received 11 August 2012 Returned for modification 28 August 2012
Accepted 10 November 2012
Published ahead of print 19 November 2012
Address correspondence to Kithiganahalli Narayanaswamy Balaji, balaji@mcbl.iisc.ernet.in.
Supplemental material for this article may be found at http://dx.doi.org/10.1128/MCB.01108-12.

doi:10.1128/MCB.01108-12

mor necrosis factor alpha (anti-TNF-α) antibody or TNF-α receptor antagonist or utilizing TNF-α-null macrophages clearly show that sustained TNF-α secretion by macrophages upon infection with *M. bovis* BCG is a critical necessity for SHH activation. The TNF-α-driven SHH signaling downregulates *M. bovis* BCG-induced Toll-like receptor 2 (TLR2) signaling events, leading to modulation of a battery of genes that regulate various functions of macrophages genes, like *Vegf-a*, *Socs-3*, *Cox-2*, and *Mmp-9*, and M1 and M2 genes. Importantly, specific microRNAs (miRNAs), miRNA 31 (miR-31) and miR-150, were identified to be the molecular regulators that bring about the negative-feedback loop comprising TLR2-SHH signaling events. SHH signaling-responsive miR-31 and miR-150 target an adaptor protein of TLR2 signaling, MyD88, leading to suppression of TLR2 responses. Thus, the current study illustrates how SHH signaling tightly regulates the kinetics and strengths of *M. bovis* BCG-specific TLR2 responses, emphasizing a novel role for SHH signaling in host immune responses to mycobacterial infections.

MATERIALS AND METHODS

Cells, mice, and bacteria. Primary macrophages were isolated from peritoneal exudates of C57BL/6 and TLR2$^{-/-}$ mice. Briefly, mice were intraperitoneally injected with 1 ml of 8% Brewer thioglycolate. After 4 days of injection, mice were sacrificed and peritoneal cells were harvested by lavage from peritoneal cavity with ice-cold phosphate-buffered saline (PBS). The cells were cultured in Dulbecco modified Eagle medium (DMEM; Gibco-Invitrogen, USA) containing 10% fetal bovine serum (FBS) for 6 to 8 h, and adherent cells were used as peritoneal macrophages. Bone marrow-derived macrophages (BMDMs) were isolated from femurs and tibias obtained from wild-type (WT) or TNF-α$^{-/-}$ mice. BMDMs were cultured in DMEM containing 30% L929 fibroblast-conditioned medium for 7 days. The purity of these cells was confirmed by F4/80 staining using fluorescence-activated cell sorting and was found to be >95%. All transfection studies were carried out with murine RAW 264.7 macrophage-like cells or human monocytic THP1 cells. Human monocytic THP1 cells were differentiated to macrophages by treatment with 5 nM phorbol myristate acetate for 18 h and rested for 3 days prior to infection or treatment. All studies involving mice were carried out after the approval from the Institutional Ethics Committee for animal experimentation, Indian Institute of Science, as well as from the Institutional Biosafety Committee, Indian Institute of Science. *M. bovis* BCG Pasteur 1173P2, *Mycobacterium smegmatis*, *Staphylococcus aureus*, *Klebsiella pneumoniae*, *Bacillus subtilis*, *Salmonella enterica*, *Shigella flexneri*, and *Escherichia coli* were grown to mid-log phase and used at a 10 multiplicity of infection (MOI) in all the experiments.

Generation and culture of human macrophages, DCs, and B cells. CD14$^+$ monocyte-derived human macrophages, dendritic cells (DCs), and CD19$^+$ B cells were obtained from healthy donors as described previously (25). Briefly, human peripheral blood mononuclear cells (PBMCs) were isolated from buffy coats of healthy donors. Monocytes were isolated from PBMCs by immunomagnetic separation using CD14$^+$ microbeads (Miltenyi Biotec, France). The purity of the monocytes was >98%. These monocytes were differentiated into macrophages or immature DCs by culturing them with L929 cell culture supernatant or interleukin-4 (IL-4; 500 IU/10^6 cells) and granulocyte-macrophage colony-stimulating factor (1,000 IU/10^6 cells), respectively, for 7 days in DMEM containing 10% FBS, 50 U/ml penicillin, 50 μg/ml streptomycin. CD19$^+$ B cells were isolated from rest of the CD14$^-$ PBMCs using a cocktail of biotinylated anti-IgG, anti-IgA, and anti-IgM antibodies (The Binding Site Limited, England), followed by immunomagnetic separation with streptavidin microbeads (Miltenyi Biotec). PBMC-derived macrophages, DCs, and B cells were infected with *M. bovis* BCG for 12 h. This study was approved by the Institutional Bioethics Committee, Indian Institute of Science.

Reagents and antibodies. General laboratory chemicals were obtained from Sigma-Aldrich (USA) or Merck (Germany). Cell culture medium was obtained from Gibco-Invitrogen. Recombinant human TNF-α, IL-1β, IL-18, and IL-6 were purchased from Peprotech. Lipopolysaccharide (LPS), R848, and CpG were purchased from Immunotools (Germany). Anti-COX-2 and anti-PCNA antibodies and TNF-α antagonist were purchased from Calbiochem (USA). Anti-β-actin antibody was purchased from Sigma-Aldrich. Anti-SHH, anti-GLI1, anti-NUMB, anti-Ser9 phospho-GSK-3β, anti-Tyr458/p55 Tyr199 phospho-p85, anti-p85, anti-Thr37/46 phospho-4EBP1, anti-α/βII Thr638/641 phospho-protein kinase C (PKC), anti-δ Thr505 phospho-PKC, anti-Thr180/Tyr182 phospho-p38 mitogen-activated protein kinase (MAPK), anti-Thr202/Tyr204 phospho-extracellular signal-regulated kinase 1/2 (ERK1/2), anti-ERK1/2, anti-suppressor of cytokine signaling 3 (anti-SOCS-3), anti-matrix metallopeptidase 9 (anti-MMP-9), and anti-MyD88 antibodies were purchased from Cell Signaling Technology (USA). Anti-TNF-α antibody was purchased from Southern Biotech. Horseradish peroxidase (HRP)-conjugated anti-rabbit IgG and anti-mouse IgG were obtained from Jackson ImmunoResearch (USA).

Treatment with pharmacological reagents. In all experiments, cells were treated with the given inhibitor for 1 h before experimental treatments with the following concentrations: LY294002 (50 μM), rapamycin (100 nM), PKCα inhibitor (50 μM), PKCβ inhibitor (20 μM), PKCδ inhibitor (10 μM), PKCε inhibitor (50 μM), PKCζ inhibitor (5 μM), U0126 (10 μM), SB203580 (20 μM), SP600125 (50 μM), BAY 11-7082 (20 μM), purmorphamine (10 μM), betulinic acid (10 μM), and TNF-α antagonist (5 μM). Dimethyl sulfoxide (DMSO) at a 0.1% concentration was used as the vehicle control. In all experiments involving pharmacological reagents, a tested concentration was used after careful titration experiments assessing the viability of the macrophages using the MTT [3-(4,5-dimethylthiazol-2-yl)-2,5-diphenyltetrazolium bromide] assay.

Enzyme immunoassay. Enzyme immunoassays were carried out in 96-well microtiter plates (Nunc) using cell-free culture supernatant. Vascular endothelial growth factor A (VEGF-A) and TNF-α enzyme-linked immunosorbent assay (ELISA) kits were purchased from Peprotech (USA) and BioLegends (USA), respectively. Sandwich ELISAs were performed as per the manufacturer's instruction. Briefly, assay plates were incubated with capture antibody at 4°C overnight. After blocking with 1% bovine serum albumin (BSA) for 1 h at 37°C, wells were incubated with cell-free supernatants for 2 h and then with biotinylated detection antibody for 2 h at 37°C. The wells were further incubated with streptavidin-HRP for 1 h at 37°C and developed with 3,3′,5,5′-tetramethylbenzidine (TMB). The absorbance was measured at 450 nm using an ELISA reader (Molecular Devices, USA).

RNA isolation and quantitative real-time RT-PCR. Macrophages were treated or infected as indicated, and total RNA from macrophages was isolated by TRI reagent (Sigma-Aldrich). Two micrograms of total RNA was converted into cDNA using a first-strand cDNA synthesis kit (Bioline, United Kingdom). Quantitative real-time reverse transcription-PCR (RT-PCR) was performed using a SYBR green PCR mixture (KAPA Biosystems, USA) for quantification of the target gene expression. All the experiments were repeated at least three times independently to ensure the reproducibility of the results. The primers used for quantitative real-time RT-PCR amplification are summarized in Table S1 in the supplemental material.

Immunoblotting. Macrophages were treated or infected as indicated and were lysed in radioimmunoprecipitation assay buffer constituting 50 mM Tris-HCl (pH 7.4), 1% NP-40, 0.25% sodium deoxycholate, 150 mM NaCl, 1 mM EDTA, 1 mM phenylmethylsulfonyl fluoride (PMSF), 1 μg/ml each of aprotinin, leupeptin, and pepstatin, 1 mM Na_3VO_4, and 1 mM NaF. In case of isolation of the nuclear fraction, the cell pellets were gently lysed in ice-cold buffer A (10 mM HEPES, pH 7.9, 10 mM KCl, 0.1 mM EDTA, 0.1 mM EGTA, 1 mM dithiothreitol [DTT], 0.5 mM PMSF). After incubation on ice for 15 min, the cell membrane was disrupted with 10% NP-40 and the nuclear pellets were recovered by centrifugation at

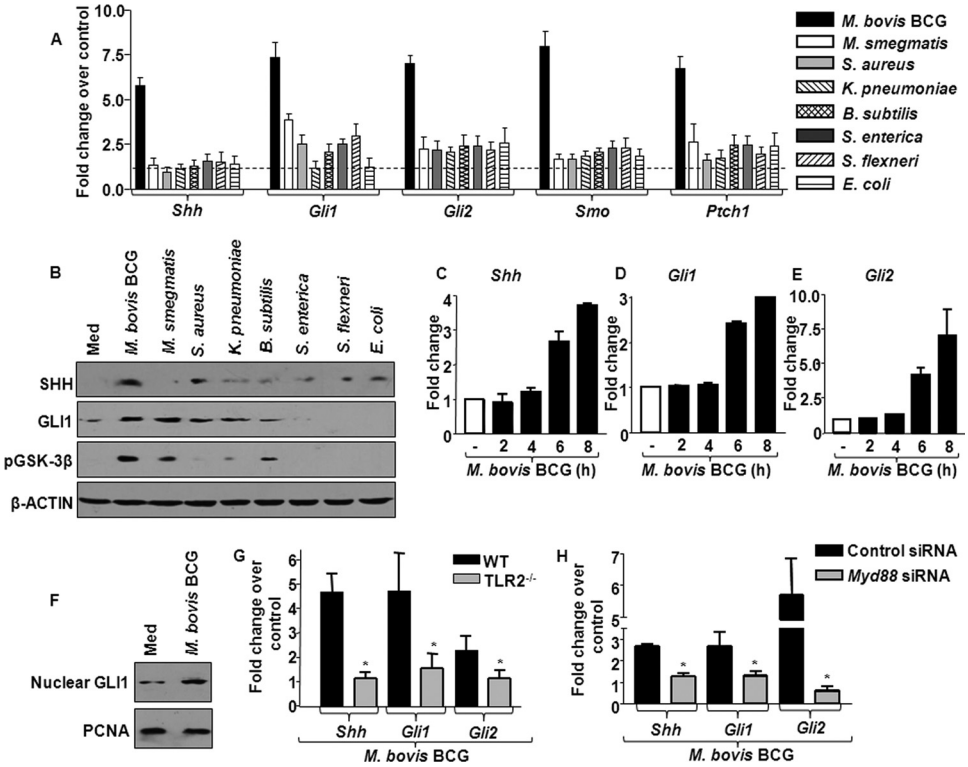

FIG 1 Among the pathogens, *M. bovis* BCG predominantly upregulates SHH signaling through TLR2. (A) Transcript analysis of SHH signaling activation markers *Shh*, *Gli1*, *Gli2*, *Smo*, and *Ptch1* upon infection of mouse peritoneal macrophages with various microbes (mean ± SE, $n = 6$). (B) Total protein levels of SHH, GLI1, and pGSK-3β were analyzed by immunoblotting. Blots are representative of 3 independent experiments with β-actin as a loading control. (C to E) Time-kinetic analysis of *Shh* (C), *Gli1* (D), and *Gli2* (E) assayed by quantitative real-time RT-PCR. (F) The activation status of SHH signaling was assessed by analyzing GLI1 in the nuclear fractions of macrophages infected with *M. bovis* BCG. (G and H) Expression of *Shh*, *Gli1*, and *Gli2* was evaluated by quantitative real-time RT-PCR in WT or TLR2-null macrophages infected with *M. bovis* BCG (G) or in *M. bovis* BCG-infected RAW 264.7 macrophages transfected with control siRNA or *Myd88* siRNA (H). Data represent means ± SEs ($n = 3$). *, $P < 0.05$ versus WT-infected macrophages or *M. bovis* BCG-infected control siRNA-transfected macrophages. $TLR2^{-/-}$, TLR2 knockout; Med, medium.

13,000 rpm for 15 min at 4°C. Nuclear pellets were lysed with ice-cold buffer C (20 mM HEPES, pH 7.9, 0.4 M NaCl, 1 mM EDTA, 1 mM EGTA, 1 mM DTT, 1 mM PMSF), and nuclear extracts were collected after centrifugation at 13,000 rpm for 20 min at 4°C. An equal amount of protein from each cell or nuclear lysate was resolved in a 12% SDS-polyacrylamide gel and transferred to polyvinylidene difluoride membranes (Millipore, USA) by the semidry transfer (Bio-Rad, USA) method. Nonspecific binding was blocked with 5% nonfat dry milk powder in TBST (20 mM Tris-HCl [pH 7.4], 137 mM NaCl, 0.1% Tween 20) for 60 min. The blots were incubated overnight at 4°C with primary antibody, followed by incubation with goat anti-rabbit HRP-conjugated or donkey anti-mouse HRP-conjugated secondary antibody in 5% BSA for 2 h. After washing in TBST, the immunoblots were developed with an enhanced chemiluminescence detection system (PerkinElmer, USA) as per the manufacturer's instruction.

Tuberculosis patients and healthy individuals. The study population was comprised of healthy individuals ($n = 7$) and pulmonary tuberculosis patients ($n = 10$) reporting to the National Institute of Mental Health and Neurosciences, Bangalore, India. Radiological and clinical examinations were performed on each of the subjects under study to confirm active tuberculosis in pulmonary tuberculosis patients and to exclude individuals with active tuberculosis disease in the case of healthy individuals. The study subjects gave written consent, and the study was approved by the Institutional Bioethics Committee.

miRNA expression profiling. The total RNA was isolated from PBMCs obtained from TB patients and healthy individuals. Using the miRCURY LNA array power labeling kit (Exiqon, Denmark), sample and reference RNAs were fluorescent labeled with Hy3 and Hy5, respectively. The hybridization of sample and reference RNAs was carried out at the Tecan HS4800 hybridization station (Tecan, Austria). The miRCURY LNA array microarray slides were scanned using a G2565BA microarray scanner system (Agilent, USA), and image analysis was performed using ImaGene (version 7.0) software (BioDiscovery, USA). The median ratio of Hy3/Hy5 intensity for replicative spots of each miRNA was calculated, and the fold change in the ratio for TB patients compared with that for the healthy individuals was plotted. Data obtained were analyzed by significance analysis of microarrays (SAM) to identify differentially regulated miRNAs. Additionally, the significant miRNAs that were identified by SAM were subjected to hierarchical clustering analysis (HCA) to identify their pattern of expression in TB patients compared with that in the healthy individuals.

Quantification of miRNA expression. For detection of miR-31, miR-150, and miR-146a by quantitative real-time RT-PCR, total RNA was isolated from infected or treated macrophages or PBMCs using the TRI reagent (Sigma-Aldrich). Quantitative real-time RT-PCR for miR-31, miR-150, and miR-146a was done using TaqMan miRNA assays (Applied Biosystems, USA) as per the manufacturer's instruction. U6 snRNA was used for normalization.

***In vivo* studies in mice.** Each *in vivo* experiment involved 6 to 8 mice per group. For intracranial inoculation, mice were first anesthetized with intraperitoneal (i.p.) injection of ketamine (6 mg). An intracerebral infection of 10^6 *M. bovis* BCG bacteria suspended in 50 μl sterile PBS was done using a 26-gauge syringe needle. Control mice received 50 μl of sterile PBS using the same protocol. After 5 days of inoculation, mouse brain was

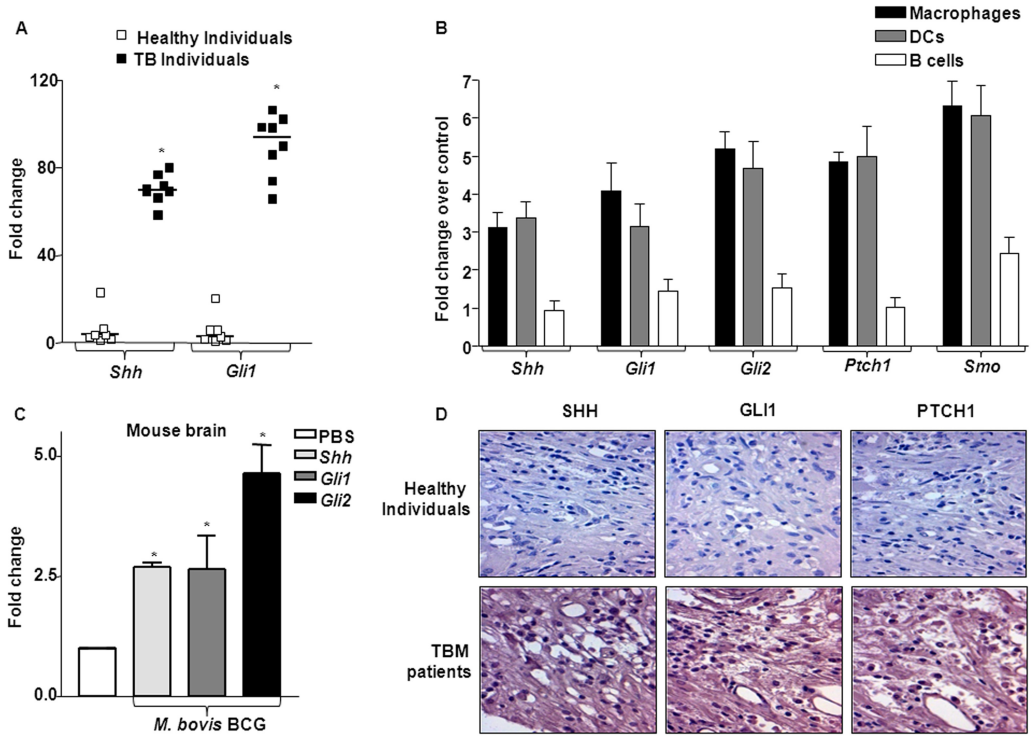

FIG 2 *In vivo* induction of SHH signaling. (A) RNA isolated from total PBMCs of healthy individuals ($n = 7$) or TB patients ($n = 7$) was used to analyze levels of *Shh*, *Gli1*, and *Gli2* transcripts. *, $P < 0.05$ compared to PBMCs of healthy individuals. (B) Macrophages, DCs, and B cells were isolated from total PBMCs of healthy individuals, followed by infection with *M. bovis* BCG. SHH signaling pathway components were assayed using quantitative real-time RT-PCR (mean ± SE, $n = 3$). (C) *M. bovis* BCG bacilli were inoculated into the cranial cavity of one set of mice ($n = 4$), while the other set received PBS as a mock infection. After 5 days of infection, mice were sacrificed and total RNA from brain tissues was isolated to investigate the status of SHH signaling using quantitative real-time RT-PCR. *, $P < 0.05$ versus mice receiving PBS. (D) Brain tissue sections obtained from healthy individuals or TB meningitis patients were stained with polyclonal antibodies against SHH, GLI1, and PTCH1 proteins. Sections were counterstained with hematoxylin-eosin.

either processed for immunohistochemical analysis or utilized for RNA analysis of the target genes. For *in vivo* expression analysis of miR-31, miR-150, and miR-146a, 10^4 *M. bovis* BCG bacteria or PBS as a vehicle control was injected intravenously into the tail vein of mice. After 7 days of infection, mice were sacrificed to collect spleen and lymph nodes. Alternatively, mice were infected intraperitoneally with 10^6 *M. bovis* BCG or anti-TNF-α antibody (0.1 mg) or TNF-α antagonist (50 μg) for 12 h and peritoneal macrophages were used for further experiments. Total RNA was isolated from the spleen and lymph nodes or the infected peritoneal macrophages, and expression levels of miR-31, miR-150, and miR-146a were analyzed by quantitative real-time RT-PCR.

MyD88 3′ UTR and mutant generation. The full-length 3′ untranslated region (UTR) of MyD88 was PCR amplified and cloned into the pmirGLO vector using restriction enzyme pair SacI and XbaI. The miR-31 or miR-150 binding sites in the 3′ UTR were mutated by nucleotide replacements through site-directed mutagenesis using the megaprimer inverse PCR method. The forward primer comprised the desired mutation, and respective reverse primers were used to generate the megaprimer. The megaprimer was in turn used to amplify the entire plasmid and generate the ΔmiR-31 and ΔmiR-150 mutants.

Transfection studies. RAW 264.7 or THP1-derived macrophage cells were transfected with 100 nM small interfering RNA (siRNA) or miRNA mimic using Oligofectamine (Invitrogen) according to the manufacturer's instructions. Transfection efficiency was found to be more than 50% in all the experiments, as determined by counting the number of siGLO lamin A/C-positive cells in a microscopic field using a fluorescence microscope. At 72 h posttransfection, the cells were treated or infected as indicated and processed for expression analysis. *Myd88*, *Shh*, *Gli1*, and control siRNAs were obtained from Dharmacon as siGENOME SMARTpool reagents, which contain a pool of four different double-stranded RNA oligonucleotides. miR-31, miR-150, miR-146a, and control mimics, miR-31 siRNA and control siRNA, and miR-150 inhibitor or control inhibitor were purchased from Ambion (USA). RAW 264.7 macrophages or THP1-derived macrophage cells were transiently transfected with dominant-negative (DN) mutant forms of TLR2, p85, PKCδ, and RAF1, the MyD88 3′ UTR construct, the MyD88 3′ UTR ΔmiR-31, or MyD88 3′ UTR ΔmiR-150 using low-molecular-weight polyethylenimine (PEI; Sigma-Aldrich). At 72 h posttransfection, the cells were treated or infected as indicated and processed for immunoblotting or luciferase analysis.

Luciferase assays. For experimental target gene validations, THP1-derived macrophage cells were transfected with the MyD88 3′ UTR construct, MyD88 3′UTR ΔmiR-31, or MyD88 3′UTR ΔmiR-150, along with the β-galactosidase vector and indicated miRNA mimics or treatments. After 72 h of transfection, cells were lysed in reporter lysis buffer (Promega) and assayed for luciferase activity using luciferase assay reagent (Promega). The results were normalized for transfection efficiencies as determined by β-galactosidase activity.

Immunohistochemistry. Microtome sections (4 μm) were obtained from formalin-fixed, decalcified, and paraffin-embedded mouse brain tissue samples. These sections were first deparaffinized, subjected to antigen retrieval by boiling in 10 mM citrate buffer (pH 6.0) for 10 min, treated with 1% H_2O_2 for 10 min, and blocked with 5% BSA for 1 h at room temperature. The tissue sections were further incubated with primary antibodies overnight. After incubation with anti-rabbit HRP-conjugated secondary antibody for 90 min, sections were stained with 0.05% diaminobenzidine (DAB) and 0.03% H_2O_2 and counterstained with hematoxylin, dehydrated, and mounted. Stained tissue sections were analyzed with a Leica DM LB microscope (Leica Microsystems, Germany). All ex-

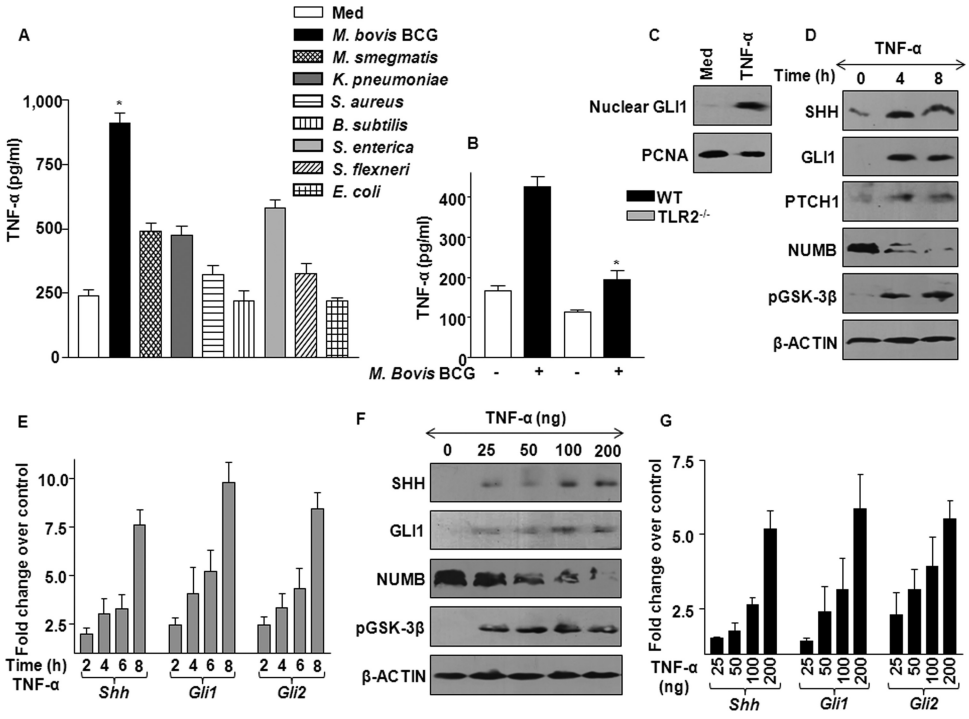

FIG 3 *M. bovis* BCG infection-induced TNF-α activates SHH signaling. (A) TNF-α protein levels were measured using ELISA. Macrophages were infected with various pathogens and nonpathogens, as shown, for 12 h, and total secreted TNF-α protein levels were measured in cell-free supernatants. The data represented were obtained from 3 separate experiments. *, $P < 0.05$ versus uninfected macrophages. (B) ELISA was performed to access secreted TNF-α from *M. bovis* BCG-infected WT and TLR2-null macrophages (mean ± SE, $n = 3$). *, $P < 0.05$ versus WT-infected macrophages. (C) The nuclear fraction from TNF-α-treated macrophages was evaluated for GLI1 nuclear translocation compared to that in untreated macrophages. Blots are representative of 3 independent experiments. (D) Macrophages were treated with TNF-α at the indicated time points, and immunoblotting was performed on total cell lysate with antibodies against SHH, GLI1, PTCH1, NUMB, and pGSK-3β. Data are for 3 independent experiments. (E) Macrophages were treated as described for panel D, and induced expression of *Shh*, *Gli1*, and *Gli2* transcripts was assayed by quantitative real-time RT-PCR analysis. These results are representative of 3 separate experiments. (F) Activation of SHH signaling with increasing doses of TNF-α treatment was assayed by immunoblotting. Equal loading of proteins was ensured by probing blots with anti-β-actin antibody. (G) Macrophages were treated as described for panel F, and *Shh*, *Gli1*, and *Gli2* transcript levels were determined using quantitative real-time RT-PCR (mean ± SE, $n = 3$).

periments were performed with appropriate isotype-matched control antibodies.

Statistical analysis. Levels of significance for comparison between samples were determined by the Student *t* test distribution and one-way analysis of variance. The data in the graphs are expressed as the mean ± standard error (SE), and *P* values of <0.05 were defined as significant. GraphPad Prism (version 3.0) software (GraphPad Software) was used for all the statistical analysis.

RESULTS

***M. bovis* BCG-specific TLR2 signaling regulates activation of SHH signaling.** The hedgehog (HH) signaling pathway, a novel regulator of cell fate decisions during embryonic development, tumorigenesis, etc., appears to exert significant effects on the initiation, progression, and perpetuation of various disease conditions. SHH, a member of the HH family of signaling molecules, often plays key roles in controlling cell fate decisions across a range of biological systems, including drosophila, mammals, etc., as well as during various other pathophysiological diseases, including cancer (26, 27). However, the important contributory role for SHH signaling during microbial infections of host macrophages and the manifestation of pathogenesis remains unclear.

In order to elucidate the role of SHH signaling during infections with microbes, macrophages were infected with representative members of pathogenic and nonpathogenic eubacteria. In this screen, *M. bovis* BCG and *M. smegmatis* were chosen from the acid-fast bacillus group, and *S. aureus*, *K. pneumoniae*, and *B. subtilis* and *S. enterica*, *S. flexneri*, and *E. coli* were selected to represent Gram-positive and Gram-negative eubacteria, respectively. Among the tested microbes, *M. bovis* BCG, a vaccine strain, elicits a robust activation of SHH signaling in macrophages compared to infection with the chosen Gram-positive or Gram-negative microbes (Fig. 1A and B). The screen involved expression-level analysis of canonical SHH signaling molecules like *Shh*, *Gli1*, *Gli2*, *Smo*, and *Ptch1*, which serve as readouts for induced SHH signaling, using real-time quantitative RT-PCR or immunoblotting. Albeit *M. bovis* BCG demonstrated a significantly higher capacity to activate SHH signaling, nonpathogenic *M. smegmatis* or selected eubacteria, irrespective of their pathogenic attributes, failed to do the same. Further, *M. bovis* BCG markedly inhibited the expression and activation of known negative regulators of SHH signaling, NUMB and GSK-3β (Fig. 1B; see Fig. S1A in the supplemental material). Kinetic analysis of expression of canonical members of SHH signaling revealed that *M. bovis* BCG induced *Shh*, *Gli1*, or *Gli2* gene expression at lower levels at early times and upregulated gene expression at later time points (Fig. 1C to E). The augmented expression of *Shh*, *Gli1*, or *Gli2* coincided with the concomitant inhibition of expression of known negative regulators of SHH signaling, NUMB and GSK-3β (see Fig. S1B in the supplemental

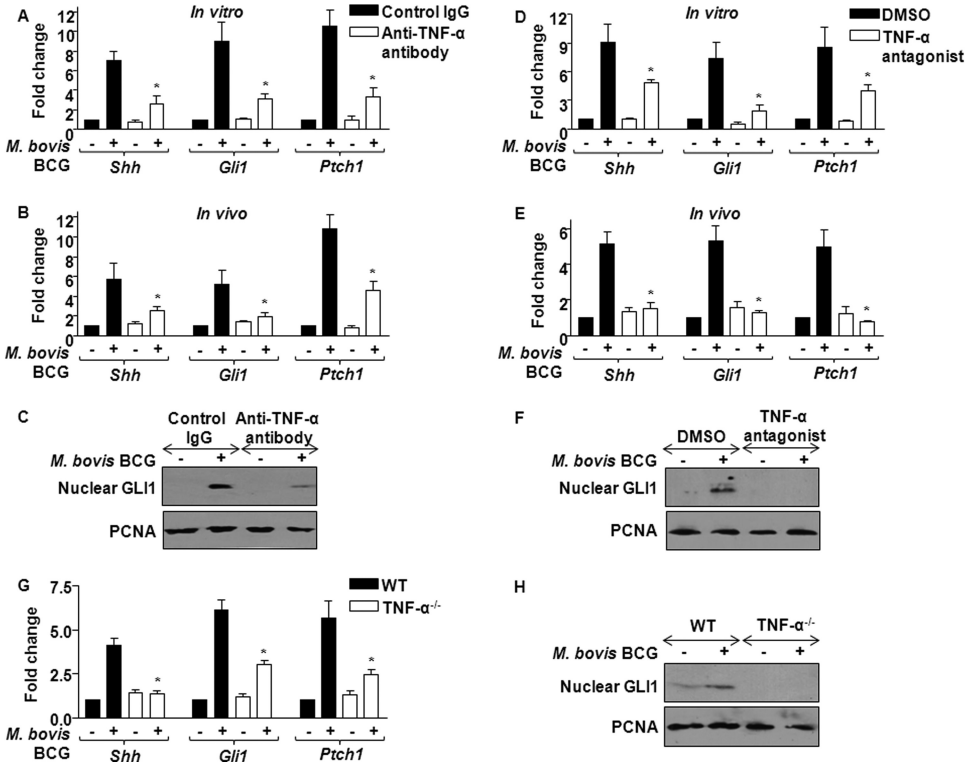

FIG 4 TNF-α is a critical mediator of *M. bovis* BCG-trigged SHH signaling. (A) Macrophages were treated *in vitro* with anti-TNF-α antibody (10 μg) 6 h prior to *M. bovis* BCG infection, and SHH signaling pathway components were monitored by quantitative real-time RT-PCR. Data represent means ± SEs ($n = 3$). *, $P < 0.05$ versus control IgG-treated *M. bovis* BCG-infected macrophages. (B) Anti-TNF-α antibody (0.1 mg) was injected i.p. into each mouse for 12 h prior to i.p. infection with *M. bovis* BCG. Peritoneal macrophages isolated were analyzed for canonical SHH signaling molecules (mean ± SE, $n = 3$). *, $P < 0.05$ versus control IgG-injected *M. bovis* BCG-infected mice. (C) The activation status of SHH signaling was ascertained by nuclear translocation of GLI1 with or without *in vitro* treatment of anti-TNF-α antibody (10 μg). Blots are representative of 3 independent experiments. (D and E) Macrophages were treated *in vitro* with 5 μg (D) or mice were injected with 0.5 mg (E) of TNF-α antagonist, and *M. bovis* BCG-induced SHH signaling induction in peritoneal macrophages was monitored using quantitative real-time RT-PCR for *Shh*, *Gli1*, and *Ptch1*. Data represent means ± SEs ($n = 3$). *, $P < 0.05$ versus control IgG-treated *M. bovis* BCG-infected macrophages or mice. (F) GLI1 nuclear translocation was assayed in macrophages treated with TNF-α antagonist with immunoblotting. DMSO was utilized as the vehicle control. (G and H) *M. bovis* BCG-induced SHH signaling was analyzed in bone marrow-derived macrophages from TNF-α-null mice or WT mice using quantitative real-time RT-PCR (G) or immunoblotting (H). Data represent means ± SEs ($n = 4$). *, $P < 0.05$ versus *M. bovis* BCG-infected WT bone marrow-derived macrophages. Blots are representative of 3 independent experiments.

material). Additionally, nuclear translocation of GLI1 and secretion of the cleaved form of SHH mark the activation of SHH signaling. As shown in Fig. 1F, *M. bovis* BCG challenge triggered the nuclear translocation of GLI1. The 19-kDa cleaved active form of SHH was detected in both the cell lysate and the corresponding supernatant obtained from *M. bovis* BCG-infected macrophages (see Fig. S1C in the supplemental material). Previously, we have demonstrated that pathogen-specific activation of TLR2 upon infection with *M. bovis* BCG, in comparison to other pathogenic microbes, including *S. enterica* serovar Typhimurium and *S. aureus*, programs macrophages for robust upregulation of Wnt–β-catenin signaling (9). In this context, macrophages from TLR2-null mice were severely compromised in their ability to trigger *M. bovis* BCG-induced expression of the effectors of canonical SHH signaling (Fig. 1G). Similarly, siRNA-mediated knockdown of *Myd88* significantly reduced *M. bovis* BCG-triggered activation of SHH signaling (Fig. 1H).

Activation of SHH signaling during *M. tuberculosis* infection. In order to bring relevance to the biology of *Mycobacterium* infection *in vivo*, we investigated the expression of SHH signaling in cells derived from tuberculosis patients. Transcript analysis demonstrated higher levels of SHH and GLI1 expression in PBMCs obtained from pulmonary TB patients (Fig. 2A). In order to evaluate the role of antigen-presenting cells other than monocytes, which represent ~10% of the PBMCs, we isolated macrophages, DCs, and B cells from PBMCs derived from healthy donors. These subsets of cells were challenged with *M. bovis* BCG, and the expression analysis of SHH signaling signatures was assayed. As illustrated in Fig. 2B, among the antigen-presenting cells, macrophages and DCs exhibited infection-driven SHH signaling, whereas B cells did not. Further, in order to delineate participation of SHH signaling in mycobacterial pathogenesis *in vivo*, we utilized a well-known mouse model of TBM, wherein mycobacterial bacilli were inoculated intracranially and progressive activation of SHH signaling was analyzed. As evidenced in Fig. 2C, augmented expression of SHH, GLI1, and GLI2 could be detected in mouse brains infected with *M. bovis* BCG. The immunohistochemical analysis of SHH, GLI1, and PTCH1 in brain tissue samples of TBM patients validated the *in vivo* induction of SHH signaling (Fig. 2D).

TNF-α is a critical link in activation of *Mycobacterium*-specific SHH signaling activation. TNF-α, a first-responder cyto-

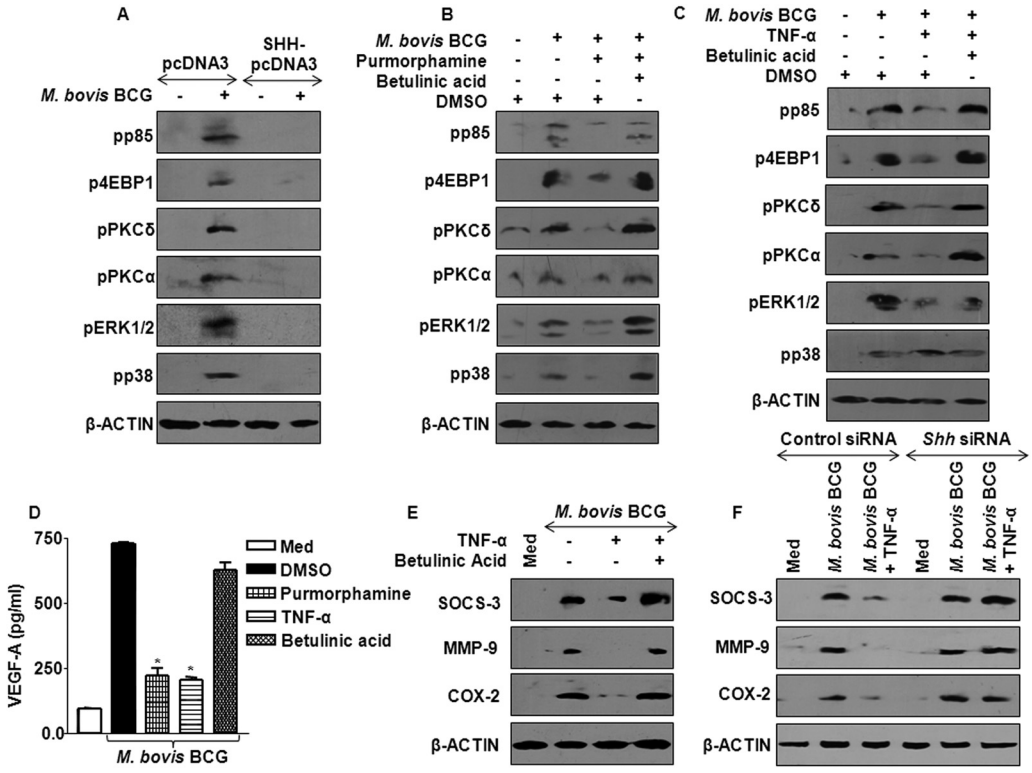

FIG 5 SHH signaling forms a feedback loop to modulate the TLR2 signaling cohort. (A) SHH was ectopically expressed in macrophages by transfection with plasmid pcDNA3-SHH. Control cells were transfected with the pcDNA3 vector alone. Immunoblotting was performed in cells overexpressing SHH or vector alone with antibodies specific to phospho-p85 (pp85), phospho-4EBP1 (p4EBP1), phospho-PKCδ (pPKCδ), phospho-PKCα (pPKCα), phospho-ERK1/2 (pERK1/2), and phospho-p38 (pp38). Blots are representative of 3 independent experiments. (B) Macrophages were treated with betulinic acid for 1 h prior to purmorphamine treatment. Cell lysates obtained from *M. bovis* BCG-infected macrophages or uninfected macrophages were analyzed using anti-pp85, anti-p4EBP1, anti-pPKCδ, anti-pPKCα, anti-pERK1/2, and anti-pp38. Blots are representative of 3 separate experiments. (C) Betulinic acid-treated macrophages were stimulated with TNF-α, followed by infection with *M. bovis* BCG. Immunoblotting was performed on equal amounts of proteins, as described for panel B. (D) Expression of VEGF-A protein in the supernatants of macrophages treated with purmorphamine, TNF-α, or betulinic acid and infected with *M. bovis* BCG assayed by sandwich ELISA. Data are the means of three replicates. *, $P < 0.05$ versus *M. bovis* BCG-infected macrophages. (E) The levels of SOCS-3, MMP-9, and COX-2 expression were monitored in macrophages pretreated with betulinic acid and stimulated with TNF-α, followed by infection with *M. bovis* BCG. DMSO was used as the vehicle control. Blots were probed with anti-β-actin antibody to ensure equal loading of proteins. Results for a representative panel of at least 3 independent experiments are shown. (F) RAW 264.7 macrophages were transfected with control siRNA or *Shh* siRNA. After 72 h of transfection, cells were stimulated with TNF-α prior to *M. bovis* BCG infection. The levels of expression of TLR2 signaling-responsive genes were assayed as discussed for panel E. Blots are representative of 3 independent experiments.

kine, is released upon infection of macrophages with various microbes, including pathogenic mycobacteria. TNF-α exhibits a critical role in host immunity during pathogenic mycobacterial infections and acts as rate-limiting factor for maintenance of granulomas (28). Importantly, pathogenic as well as nonpathogenic mycobacteria elicit differential levels of TNF-α secretion by macrophages. Further, a recent study demonstrates that TNF-α-mediated regulation of NOTCH signaling by inhibiting NUMB expression is involved in the suppression of FOXA2 transactivation activity (29). Since NUMB is a known negative regulator of SHH signaling, we explored the contribution of TNF-α in *M. bovis* BCG's ability to induce SHH signaling in macrophages by modulating NUMB activity. As shown in Fig. 3A and B, among the tested microbes, *M. bovis* BCG infection of macrophages resulted in sustained production of TNF-α in a TLR2-dependent manner. Interestingly, TNF-α holds the capacity to activate SHH signaling, as evidenced by GLI1 nuclear translocation (Fig. 3C). To test the sufficiency of TNF-α to drive SHH signaling, we analyzed the kinetics of SHH signaling activation in macrophages at different time points as well as at various concentrations of TNF-α (Fig. 3D to G). The induced expression of SHH, GLI1, GLI2, and PTCH1 at the transcript or protein levels with a concomitant decrease in NUMB or increased phosphorylation of GSK-3β advocates for a direct correlation between *M. bovis* BCG-induced TNF-α and robust activation of SHH signaling. Importantly, similar to results obtained with *M. bovis* BCG infection (Fig. 1C to E), TNF-α treatment induced SHH, GLI1, GLI2, and PTCH1 expression at lower levels at early times, and expression was upregulated at later time points. To validate the role of *M. bovis* BCG-driven production of TNF-α in inducing SHH signaling, macrophages were pretreated with neutralizing anti-TNF-α antibody or TNF-α receptor antagonist *in vitro*, followed by infection with *M. bovis* BCG. Similarly, mice were pretreated with anti-TNF-α antibody or TNF-α receptor antagonist, followed by infection with *M. bovis* BCG. As shown in Fig. 4A to F, neutralization of TNF-α or blockade of TNF-α receptor signaling significantly reduced the infection-induced SHH signaling activation. Importantly, macrophages derived from TNF-α-

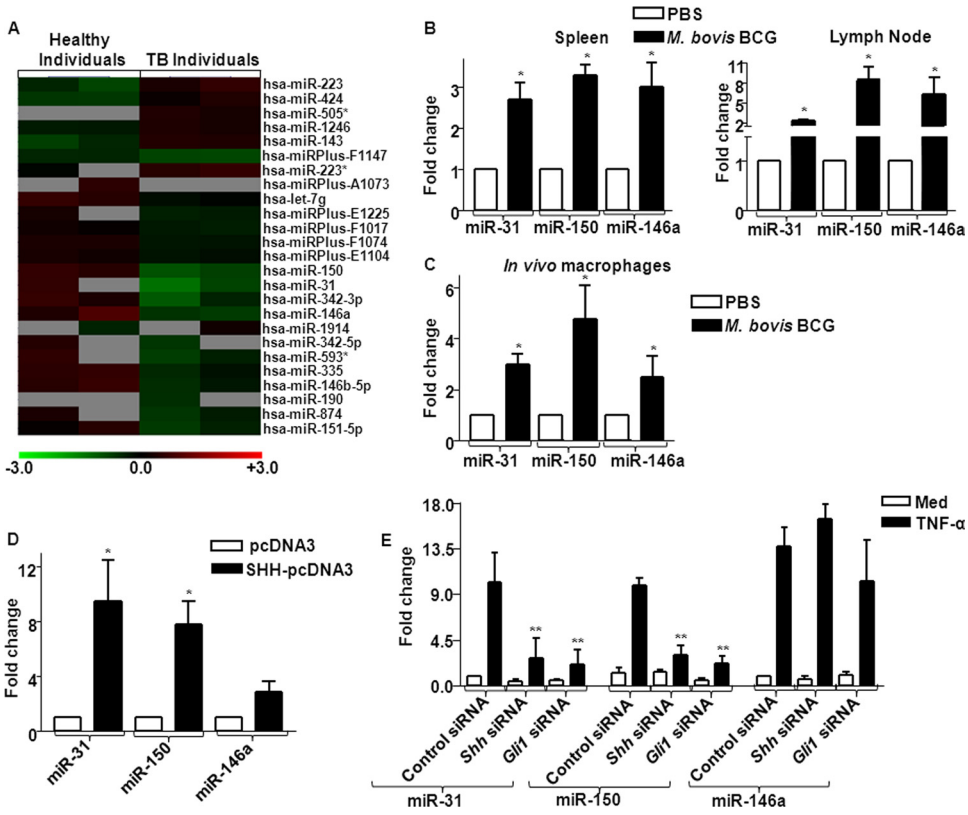

FIG 6 Modulation of miR-31, miR-150, and miR-146a during mycobacterial infection. (A) Genome-wide miRNA microarray profiling was done in PBMCs from TB patients or healthy individuals. A heat map of the profile in TB patients ($n = 4$) compared with that in healthy individuals ($n = 4$) is shown. (B) Mice were intravenously challenged with *M. bovis* BCG for 5 days, and levels of miR-31, miR-150, and miR-146a expression in spleen and lymph nodes were analyzed by quantitative real-time RT-PCR. *, $P < 0.05$ compared to PBS-injected or uninfected mice. (C) Mice were i.p. infected with *M. bovis* BCG *in vivo*, and total levels of miR-31, miR-150, and miR-146a expression were assayed as described for panel B. *, $P < 0.05$ versus PBS-injected or uninfected mice. (D) SHH was overexpressed in macrophages, and levels of miR-31, miR-150, and miR-146a expression were assayed using quantitative real-time RT-PCR. *, $P < 0.05$ versus pcDNA3-transfected macrophages. (E) Knockdown of SHH and GLI1 was achieved by transfecting specific siRNAs in macrophages, while the mock-treated set received nontargeted control siRNAs. Quantitative real-time RT-PCR analysis was performed on total RNA isolated from either TNF-α-treated or untreated cells using miR-31-, miR-150-, and miR-146a-specific primers. Results of a representative panel of 3 independent experiments are shown. *, $P < 0.05$ compared to TNF-α-treated cells with control siRNA.

null mice significantly compromised *M. bovis* BCG's ability to induce SHH signaling (Fig. 4G and H).

In order to address if TNF-α-induced SHH operates in an autocrine or paracrine manner, cycloheximide, a well-known protein translational inhibitor, was utilized to pretreat macrophages, followed by infection with *M. bovis* BCG. The data presented in Fig. S2A in the supplemental material clearly demonstrate that *M. bovis* BCG-triggered TNF-α mRNA expression was unaffected by cycloheximide. However, cycloheximide reduced *M. bovis* BCG-induced *Shh*, *Gli1*, and *Ptch1* mRNA levels, implicating the crucial role/necessity of a secretory TNF-α in mediating *M. bovis* BCG-induced SHH signaling. Thus, these results present an interesting dichotomy of SHH signaling in utilizing both autocrine and paracrine attributes to orchestrate *M. bovis* BCG-driven macrophage function. Further, to address the ability of other inflammatory cytokines, such as IL-1, IL-6, and IL-18, to induce SHH signaling activation, macrophages were treated with recombinant TNF-α, IL-1β, IL-6, or IL-18 and examined for the induction of SHH signaling. Among these inflammatory cytokines, TNF-α exhibited robust induction of SHH signaling. Interestingly, while IL-18 triggered moderate induction of SHH signaling, IL-1β and IL-6 failed to induce transcript expression of *Shh*, *Gli1*, *Gli2*, *Ptch1*, and *Smo* (see Fig. S2B in the supplemental material). However, only TNF-α could activate SHH signaling, as monitored by GLI1 nuclear translocation (see Fig. S2C in the supplemental material).

SHH signaling acts as negative-feedback loop to restrict TLR2 responses during mycobacterial infection. Macrophages often tailor innate immunity to microbial pathogens by careful orchestration of signaling events triggered by TLR2. From a broader perspective, TLR2 receptor engagement with mycobacteria, including *M. bovis* BCG, has a direct bearing on cell fate decisions through diligent regulation of a wide range of cellular genes that modulate both innate and adaptive immune responses (see Fig. S3A and B in the supplemental material). As described in Fig. 1C to E and Fig. 3D and G, time-kinetic analysis demonstrated that *M. bovis* BCG-induced as well as infection-stimulated TNF-α-induced *Shh*, *Gli1*, and *Gli2* expression was significantly augmented at later time points. In this regard, we explored whether TNF-α-driven late-phase activation of SHH signaling could act as a feedback-signaling loop to fine-tune and regulate prolonged TLR2-driven responses. The enforced expression of SHH in macrophages resulted in downregulation of *M. bovis* BCG-induced

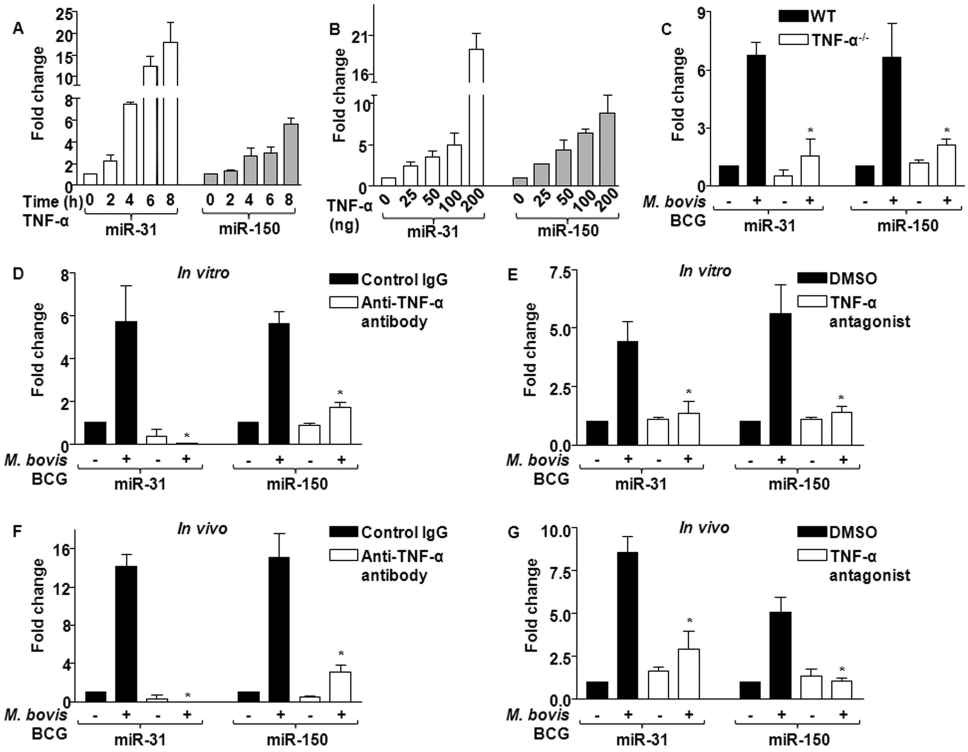

FIG 7 TNF-α regulates miR-31 and miR-150 expression during mycobacterial infection. (A and B) *In vitro* kinetics of miR-31 and miR-150 expression in macrophages treated with TNF-α at the indicated time points (A) and different concentrations (B) are shown (mean ± SE, $n = 3$). (C) TNF-α-null and WT bone marrow-derived macrophages were infected with a 1:10 MOI of *M. bovis* BCG to analyze the expression of miR-31 and miR-150. Data represent means ± SEs ($n = 4$). *, $P < 0.05$ versus *M. bovis* BCG-infected WT bone marrow-derived macrophages. (D and E) Macrophages were treated *in vitro* with either anti-TNF-α antibody (10 μg) (D) or TNF-α antagonist (5 μg) (E), and the levels of *M. bovis* BCG-induced miR-31 and miR-150 expression were assayed by quantitative real-time RT-PCR (mean ± SE, $n = 4$). *, $P < 0.05$ compared to *M. bovis* BCG-infected control IgG-treated/DMSO-treated cells. (F and G) Mice were i.p. injected with either anti-TNF-α antibody (0.1 mg) or TNF-α antagonist (0.5 mg) 6 h prior to *M. bovis* BCG i.p. infection. The levels of miR-31 and miR-150 expression analyzed were similar to those shown in panels D and E (mean ± SE, $n = 4$). *, $P < 0.05$ compared to *M. bovis* BCG-infected control IgG/DMSO-treated mice.

phosphoinositide 3-kinase (PI3K), PKCα, ERK1/2, or p38 MAPK activation (Fig. 5A). Further, treatment of macrophages with purmorphamine, a pharmacological activator of SHH signaling that leads to constitutive activation of SMO, considerably suppressed *M. bovis* BCG-dependent TLR2-mediated PI3K, PKCα, ERK1/2, or p38 MAPK activation (Fig. 5B). Pharmacological perturbations of TNF-α-induced SHH signaling by betulinic acid, a known inhibitor of GLI activity, rescued *M. bovis* BCG's ability to activate PI3K-PKC and MAPK activation (Fig. 5C). Accordingly, expression of the *M. bovis* BCG-TLR2-signaling target gene *Vegf-A*, *Socs-3*, *Mmp-9*, or *Cox-2* was markedly reduced upon activation of SHH signaling by purmorphamine or TNF-α. Importantly, pharmacological inhibition of SHH signaling by betulinic acid could rescue the loss of VEGF-A, SOCS-3, MMP-9, or COX-2 or TLR2 signaling (Fig. 5D and E; see Fig. S3C in the supplemental material). Additionally, experiments utilizing *Shh* siRNA to block SHH signaling were performed to monitor TLR2 downstream signaling targets. As shown in Fig. 5F and in Fig. S3D in the supplemental material, similar to betulinic acid, knockdown of SHH signaling alleviates TNF-α-mediated suppression of TLR2 downstream signaling targets, such as VEGF-A, COX-2, SOCS-3, and MMP-9. Thus, these results strongly signify a role for *M. bovis* BCG-stimulated SHH signaling in exerting an integrated negative-feedback loop to fine-tune and regulate *Mycobacterium*-specific TLR2 responses.

SHH signaling-driven miR-31 and miR-150 target MyD88. Next, we asked how *M. bovis* BCG/TNF-α-induced SHH signaling regulates TLR2 responses. Regulation of innate receptor-triggered signaling networks often requires various checks and balances that are arbitrated by posttranscriptional control mechanisms like those mediated by miRNAs (30). Importantly, we have recently demonstrated a novel role for miR-155 in orchestrating cellular reprogramming during immune responses to mycobacterial infection (31). In this regard, we carried out genome-wide expression profiling of miRNAs in PBMCs from TB patients. The profiling identified a number of differentially regulated miRNAs between TB patients and healthy subjects; among these, our investigation focused on expression patterns of significantly deregulated miR-31, miR-150, and miR-146a (Fig. 6A). Importantly, mice challenged *in vivo* with *M. bovis* BCG exhibited enhanced expression of miR-31, miR-150, and miR-146a in spleen, lymph nodes, or peritoneal macrophages in a TLR2-dependent manner (Fig. 6B and C; see Fig. S4A and B in the supplemental material). Next, we assessed whether *M. bovis* BCG-induced TNF-α is involved in modulation of miR-31, miR-150, and miR-146a expression. As mentioned above for the data shown in Fig. 5, SHH signaling considerably suppressed *M. bovis* BCG-TLR2-mediated PI3K, PKCα, ERK1/2, or p38 MAPK activation or expression of TLR2-responsive genes. In this perspective, the gain-of-function and loss-of-function studies utilizing overexpression of SHH or

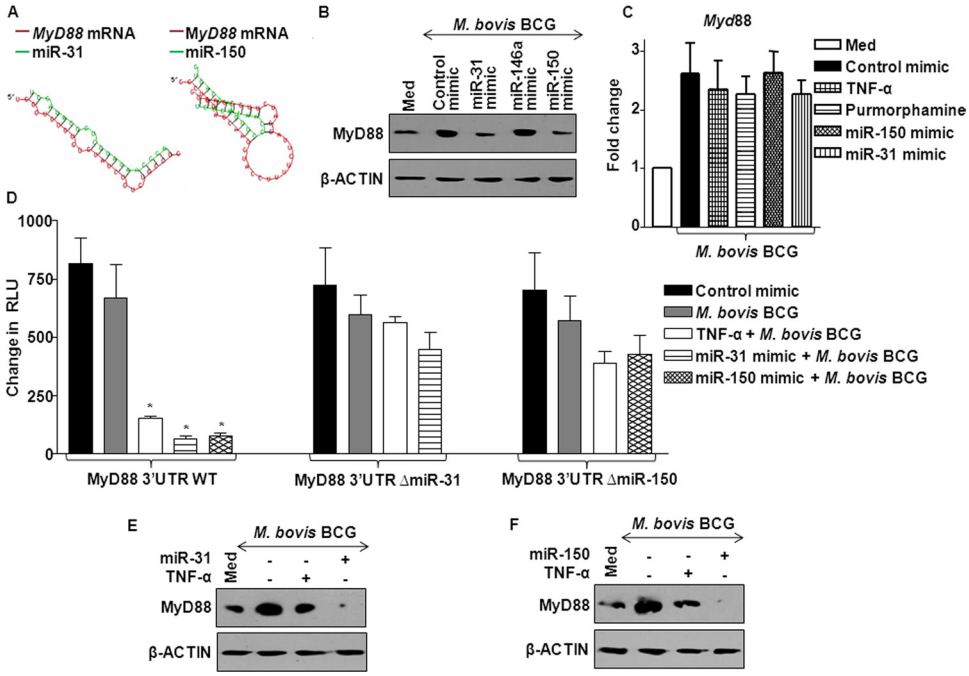

FIG 8 SHH signaling-responsive miR-31 and miR-150 target MyD88 to suppress TLR2 signaling. (A) Hybridization analysis of 3′ UTR of MyD88 with mature oligonucleotide sequences of miR-31 and miR-150 using RNAhybrid software. The structures with minimum free energy are shown. (B) miR-31, miR-146a, and miR-150 were overexpressed in macrophages by transfecting respective mimics, and levels of MyD88 expression were assayed by immunoblotting using anti-MyD88 antibody. Data are representative of 3 independent experiments. (C) The level of *Myd88* transcript expression was monitored under the indicated conditions by real-time quantitative RT-PCR using *Myd88*-specific primers. Data represent means ± SEs ($n = 3$). (D) THP1-derived macrophage cells were transfected with the WT MyD88 3′ UTR luciferase construct or MyD88 3′ UTR ΔmiR-31 or MyD88 3′ UTR ΔmiR-150 luciferase constructs along with miR-31 or miR-150 mimics, as indicated. At 72 h posttransfection, TNF-α treatment or *M. bovis* BCG infection was done as shown and luciferase assay was performed. Data represent means ± SEs ($n = 3$). RLU, relative light units. *, $P < 0.05$ versus control. (E and F) The level of MyD88 protein in macrophages was assessed either with TNF-α treatment or with overexpression of miR-31 (E) or miR150 (F). Results of a representative MyD88 immunoblotting analysis of 3 separate experiments are shown.

siRNA to *Shh* and *Gli1* validated the role for TNF-α-mediated SHH signaling in the expression of miR-31and miR-150 at later time points (Fig. 6D and E; see Fig. S4C to E in the supplemental material). However, the activated SHH signaling was dispensable for the regulation of miR-146a expression (Fig. 6D and E). Importantly, *M. bovis* BCG-induced *Shh*, *Gli1*, or *Gli2* was expressed at lower levels at early times and was upregulated at later time points during infection of macrophages (Fig. 1C and E). Consistent with these observations, TNF-α-induced expression of miR-31 and miR-150 followed a similar pattern of expression as SHH signaling activation at later time points (Fig. 7A and B). Intriguingly, *M. bovis* BCG failed to trigger the induction of miR-31 and miR-150 in TNF-α-null macrophages or in macrophages or mice that were pretreated with anti-TNF-α antibody or TNF-α receptor antagonist (Fig. 7C to G). Further, we assessed the function of miR-31 and miR-150 in fine-tuning of TLR2 responses during *M. bovis* BCG infection. The extensive bioinformatic analyses, including RNA-hybrid analysis, suggested that MyD88, an adaptor molecule important for signaling by many TLRs, is a target for miR-31 and miR-150 (Fig. 8A). The target sites located at residues spanning residues 152 to 178 (for miR-31) and residues 1598 to 1637 (for miR-150) in *Myd88* mRNA are critical for miRNA-3′ UTR interactions.

miR-31 and miR-150 modulate TLR2 responses by targeting MyD88. MyD88, as a key anchor adaptor, plays regulatory roles by integrating various signaling events generated by receptor engagement of TLRs. Importantly, MyD88 recruitment to TLR2 results in active recruitment of the p85 regulatory subunit of PI3K, leading to activation of the PI3K pathway (32, 33). As described, activation of the PI3K pathway leads to modulation of NF-κB through a strong collaboration between PKC and MAPK signaling cascades, which culminates in augmented expression of TLR2-responsive genes (9, 10, 15, 18). In this regard, enforced expression of miR-31 and miR-150, but not miR-146a, resulted in a marked reduction of *M. bovis* BCG-induced MyD88 expression in a concentration-dependent manner (Fig. 8B). However, infection-induced *Myd88* transcript levels remain unperturbed by ectopic expression of miR-31 or miR-150 (Fig. 8C). Next, we utilized the WT MyD88 3′ UTR and miR-31 and miR-150 binding-site mutants of the MyD88 3′ UTR to validate MyD88 as a direct target of miR-31 and miR-150. As shown in Fig. 8D, TNF-α treatment or cotransfection with miR-31 or miR-150 mimics markedly reduced WT MyD88 3′ UTR luciferase activity. However, repression of luciferase activity was not observed when mutant MyD88 3′ UTR luciferase constructs (for miR-31 or miR-150 binding sites) were utilized (Fig. 8D). These results strongly advocate for the possibility and validate that MyD88 is a direct target of miR-31 and miR-150. Similarly, TNF-α treatment or enforced expression of miR-31 or miR-150 significantly reduced *M. bovis* BCG-TLR2-driven MyD88 expression (Fig. 8E and F). Further, as shown in Fig. 9A, expression of miR-31 and

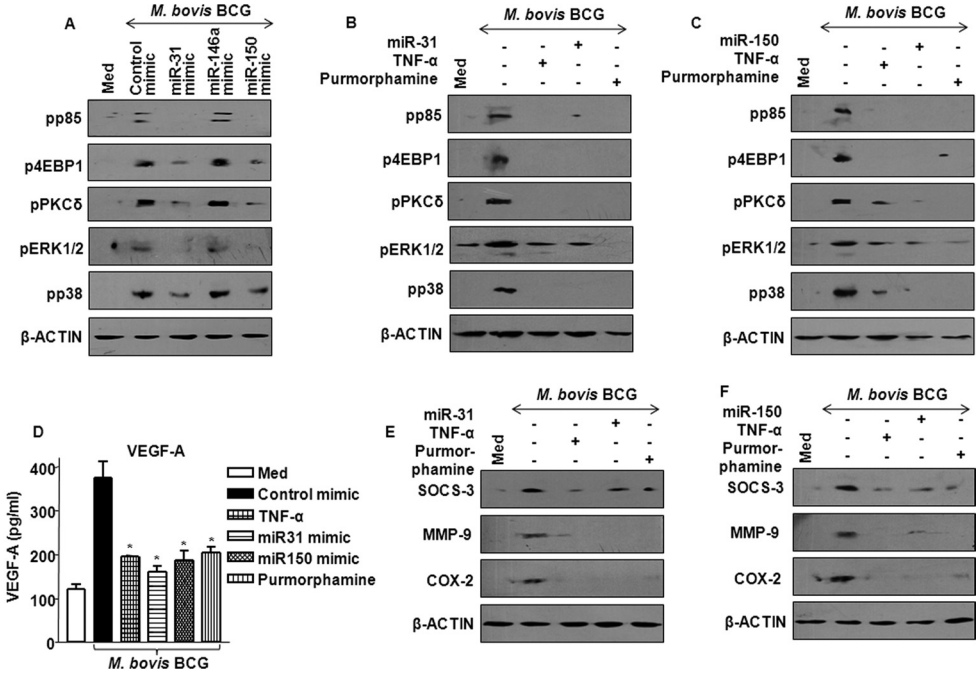

FIG 9 TLR2 responses are under the control of miR-31- and miR-150-mediated regulation. (A) miR-31, miR-146a, and miR-150 were overexpressed in macrophages by transfecting the respective mimics, which were infected with *M. bovis* BCG. Immunoblot analysis of the cell lysates using antibodies specific for phospho-p85 (pp85), phospho-4EBP1 (p4EBP1), phospho-PKCδ (pPKCδ), phospho-ERK1/2 (pERK1/2), and phospho-p38 (pp38) is shown. A representative blot of 3 replicates is shown. (B and C) miR-31 or miR-150 was ectopically expressed in macrophages by transfecting either the miR-31 mimic (B) or miR-150 mimic (C). Macrophages were subsequently stimulated with TNF-α or purmorphamine prior to *M. bovis* BCG infection. Representative results of the immunoblot analysis with the cell lysates are shown. (D) Sandwich ELISA was performed using the culture supernatants of *M. bovis* BCG-infected macrophages that were transfected or treated as indicated. Data represent means ± SEs ($n = 3$). *, $P < 0.05$ versus *M. bovis* BCG-infected macrophages. (E and F) Immunoblot analysis was performed with cell lysates of *M. bovis* BCG-infected or TNF-α- or purmorphamine-treated or macrophages transfected with miR-31 mimics (E) or miR-150 mimics (F). Representative panels of 3 independent experiments are shown.

miR-150, but not miR-146a, mimics in macrophages strongly repressed *M. bovis* BCG-driven TLR2 signaling, as evidenced by the activation status of p85 PI3K, 4EBP1, PKCδ, ERK1/2, and p38 MAPKs. Accordingly, miR-31 or miR-150 significantly reduced *M. bovis* BCG-induced activation of p85 PI3K, 4EBP1, PKCδ, ERK1/2, and p38 MAPK signaling (Fig. 9B and C). These results are in agreement with the inhibitory effects on macrophages mediated by TNF-α or purmorphamine, an activator of SHH. Importantly, miR-31 or miR-150 inhibited expression of infection-induced TLR2-responsive genes *Vegf-A*, *Socs-3*, *Mmp-9*, and *Cox-2*, similar to the effects of TNF-α or purmorphamine (Fig. 9D to F). However, transfection of macrophages with miR-31 siRNA or miR-150 inhibitor did not demonstrate a significant change in *M. bovis* BCG-driven inflammatory gene expression (see Fig. S5 in the supplemental material). These results strongly advocate for the regulatory role of TNF-α/SHH-triggered miR-31 and miR-150.

Significantly, VEGF-A- and COX-2-derived prostaglandin E_2 influences the polarization of macrophages toward an alternatively activated or M2 phenotype (34). Similarly, SOCS-3 acts as a negative regulator of signaling induced by several cytokines and Toll-like receptors, thus exhibiting a significant bearing on polarization of macrophages (18). In this regard, we assessed whether SHH-driven miR-31 and miR-150 influence the determination of M1 versus M2 polarization of macrophages. In a TLR2-dependent manner, *M. bovis* BCG triggers the expression of various M1 (*Inos*, *Tnf*-α, *Il-6*, *Il-12*, *Ccl5*, and *Cxcl9*) and M2 (*Il-10*, *Arg-1*, *Ho-1*, and *Ccl17*) genes that play critical roles in the determination of M1 versus M2 polarization of macrophages (Fig. 10A; see Fig. S6A in the supplemental material). Enforced expression of miR-31 or miR-150 significantly reduced *M. bovis* BCG-TLR2-driven expression of *Inos*, *Tnf*-α, *Il-6*, *Il-12*, *Ccl5*, *Cxcl9*, *Arg-1*, *Ho-1*, and *Ccl17* (Fig. 10B; see Fig. S6B in the supplemental material). Interestingly, we could observe different degrees of suppression of M1/M2 markers by miR-31/miR-150. On the contrary, knockdown of miR-31 and miR-150 led to a marginal increase in the levels of expression of inflammatory genes (Fig. 10C and D; see Fig. S6C to D in the supplemental material). However, extensive time-kinetics analysis did not reveal any definitive signatures of macrophage polarization. Together, these results identify a balancing act of SHH signaling-activated miR-31 and miR-150 in fine-tuning a defined set of effector functions of macrophages during *Mycobacterium*-specific TLR responses.

DISCUSSION

Our investigations identify a unique role for SHH signaling in regulating innate recognition of *M. bovis* BCG among various microbial pathogens by macrophages. Importantly, identification of SHH signaling as a recognition module that effectively regulates miR-31 and miR-150 targeting of various TLR2 responses shows that it constitutes a significant check and balance that shapes the course of mycobacterial infection. In this context, we show for the first time that *Mycobacterium*-specific TLR2 signaling effectuates rapid enrichment of the proinflammatory cytokine milieu of

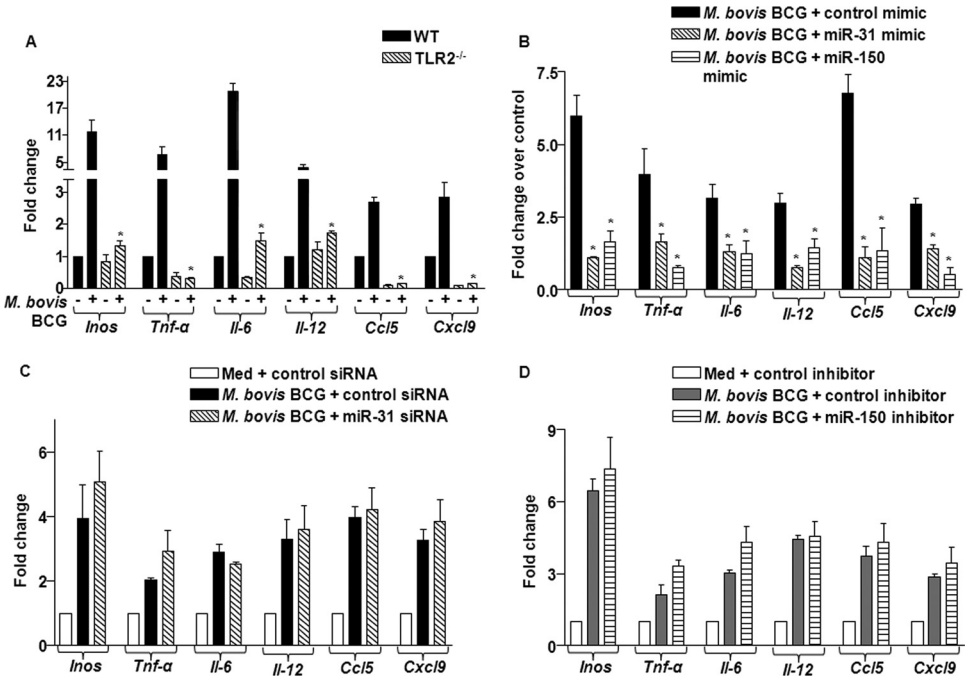

FIG 10 miR-31 and miR-150 control TLR2-responsive inflammatory gene expression. (A) WT and TLR2-null macrophages were infected with *M. bovis* BCG for 12 h. Total RNA was isolated, and the levels of *Inos*, *Tnf*-α, *Il-6*, *Il-12*, *Ccl5*, and *Cxcl9* transcript expression were analyzed using quantitative real-time RT-PCR. Data represent means ± SEs ($n = 3$). *, $P < 0.05$ versus WT *M. bovis* BCG-infected cells. (B) Macrophages were transfected with the control mimic, miR-31 mimic, or miR-150 mimic for 72 h. After *M. bovis* BCG infection for 24 h, expression of *Inos*, *Tnf*-α, *Il-6*, *Il-12*, *Ccl5*, and *Cxcl9* was analyzed using quantitative real-time RT-PCR (mean ± SE, $n = 3$). *, $P < 0.05$ versus *M. bovis* BCG-infected cells. (C and D) Macrophages were transfected with control siRNA or miR-31 siRNA (C) or with control inhibitor or miR-150 inhibitor (D). After 72 h of transfection, cells were infected with *M. bovis* BCG for 24 h, and expression of the indicated genes was analyzed using quantitative real-time RT-PCR. Data represent means ± SEs ($n = 3$).

TNF-α to induce strong SHH signaling activation both *in vitro* and *in vivo*. Activation of PKC/MAPK is requisite for SHH signaling (35), and TNF-α-induced NF-κB modulates SHH signaling (36). Our work herein further implies the role of TLR2 signaling in orchestrating SHH activation through the infection-induced TNF-α. Besides the numerous developmental functions attributed to SHH signaling, the present study has delineated the very role of such an indispensable signaling pathway in immune cells like macrophages so that they may carry out their functions effectively.

TLR2-mediated signaling events constitute a number of tight negative-feedback regulations that in turn subdue the downstream effectors of the pathway (37–40). Latest in the list are the miRNAs that fine-tune the initiation, amplification, as well as kinetics of immune responses of macrophages or dendritic cells triggered by various TLRs, including TLR2 (41). Further, miRNAs regulate several cellular processes, including the efficiency and polarization of pathogen-specific inflammatory responses (42). In this regard, whole-genomic miRNA expression profile analysis demonstrated significant deregulation of miR-31, miR-146a, and miR-150 in tuberculosis patients, which could advocate for a potential role in fine-tuning of host immune responses. Accordingly, *in vivo* and *in vitro* experiments demonstrated that miR-31 and miR-150, but not miR-146a, are *M. bovis* BCG/TNF-α-driven SHH responsive. Emphasizing the temporal regulation, the coincidence of elevated levels of miR-31 and miR-150 with the TNF-α-induced SHH signaling at the later time points provided a cue for the potential existence of a negative-feedback loop (Fig. 11).

Importantly, miR-31 and miR-150, but not miR-146a, target MyD88, an adaptor of TLR2 signaling. In this perspective, our results constitute *M. bovis* BCG-induced SHH signaling to be a fine-tuner of pathogen-specific TLR2 signaling events that eventually calibrate as well as account for crucial determinants that shape the course of infection. Interestingly, mycobacteria are known to suppress the ability of infected cells to exhibit strong immune responses. For example, infection of macrophages prior to treatment with LPS, a TLR4 agonist, blocked the macrophage responsiveness to TNF-α production (25). Similarly, *M. avium* subsp. *paratuberculosis* infection of monocytes showed a marked suppression of classical TLR9-mediated responses (43). Further, *M. tuberculosis* infection led to suppression of T-cell responses and apoptosis of *Mycobacterium*-specific $CD4^+$ T cells *in vivo* (44, 45). Similarly, *M. bovis* BCG infection led to a significant reduction of TLR4 and TLR7/8 ligand-driven expression of an antimicrobial peptide (cathelicidin), a lysosomal aspartyl protease (cathepsin D), and IL-6 (see Fig. S7 in the supplemental material). Notably, these TLR-responsive genes play important roles in cell fate decisions, including clearance of pathogens.

Taken together, our findings suggest that *M. bovis* BCG-induced TNF-α/SHH-driven miR-31 and miR-150 regulate the TLR2 responses, as exemplified by the downstream effectors VEGF-A, SOCS-3, MMP-9, and COX-2, as well as inducible nitric oxide synthase (iNOS), TNF-α, IL-6, IL-12, CCL5, CXCL9, IL-10, ARG-1, HO-1, and CCL17. However, it is interesting to observe various degrees of suppression of TLR2-responsive M1/M2 genes with the expression of miR-31 and miR-150, emphasizing the sig-

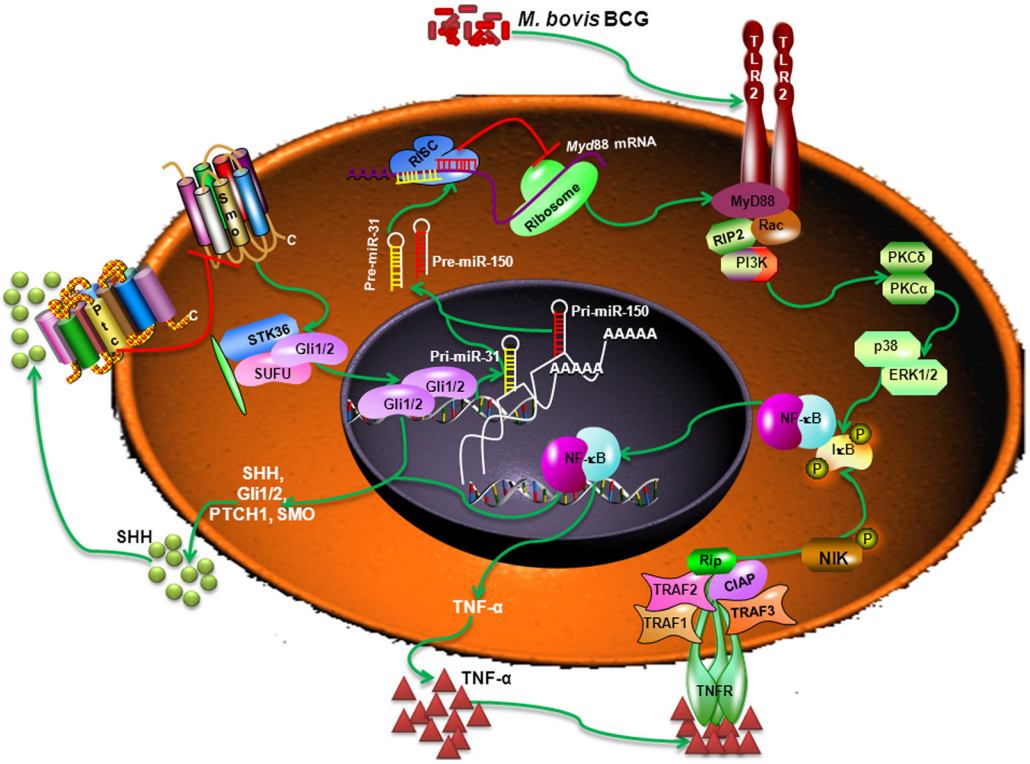

FIG 11 Model. *M. bovis* BCG, among most of the common bacterial pathogens, predominantly activates SHH signaling through stimulation of the TLR2 signaling pathway. The PI3K/PKC/MAPK signaling cohort holds the capacity to activate NF-κB, which leads to upregulation of SHH, GLI1/2, SMO, and PTCH1. The robust production of TNF-α by *M. bovis* BCG-infected macrophages amplifies SHH signaling activation to constitute a feedback loop which plays a central role in orchestrating TLR2 responses via miR-31- and miR-150-targeted MyD88. RISC,RNA-induced silencing complex; TNFR, TNF-α receptor.

nificance of fine-tuning of signals to determine the outcome of the infection. Importantly, the molecular regulators identified in the present study, SHH effectors as well as miR-31 and miR-150, can fuel the search for attractive and effective drug targets to combat diseases of the hour, like tuberculosis.

ACKNOWLEDGMENTS

We thank the Central Animal Facility, Indian Institute of Science (IISc), for providing mice for experimentation. We acknowledge Kushagra Bansal for critical comments and timely help. We sincerely thank Douglas Golenbock, University of Massachusetts Medical School, Worcester, MA, and Jae-Won Soh, Inha University, South Korea, for TLR2 DN and PKCα DN constructs, respectively. We acknowledge Kumaravel Somasundaram and Utpal Nath of the Indian Institute of Science, Bangalore, India, for help during the current study.

This study is supported by funds from the Department of Biotechnology, Department of Science and Technology (DST), Council for Scientific and Industrial Research (CSIR), and Indian Council of Medical Research (ICMR), Government of India, and the Indo-French Center for Promotion of Advanced Research (CEFIPRA) (reference number 4803-1). Infrastructure support from ICMR (Center for Advanced Study in Molecular Medicine), DST (FIST), and UGC (special assistance, to K.N.B.) and fellowships from CSIR (to D.S.G.) and IISc (to S.H.) are acknowledged.

We declare no conflict of interest.

REFERENCES

1. **Bergeron SA, Milla LA, Villegas R, Shen MC, Burgess SM, Allende ML, Karlstrom RO, Palma V.** 2008. Expression profiling identifies novel Hh/Gli-regulated genes in developing zebrafish embryos. Genomics **91**:165–177.
2. **Lin SL, Chang SJ, Ying SY.** 2006. Transcriptional control of Shh/Ptc1 signaling in embryonic development. Gene **367**:56–65.
3. **Le H, Kleinerman R, Lerman OZ, Brown D, Galiano R, Gurtner GC, Warren SM, Levine JP, Saadeh PB.** 2008. Hedgehog signaling is essential for normal wound healing. Wound Repair Regen. **16**:768–773.
4. **Crompton T, Outram SV, Hager-Theodorides AL.** 2007. Sonic hedgehog signalling in T-cell development and activation. Nat. Rev. Immunol. **7**:726–735.
5. **Gianakopoulos PJ, Skerjanc IS.** 2005. Hedgehog signaling induces cardiomyogenesis in P19 cells. J. Biol. Chem. **280**:21022–21028.
6. **Ahmed RK, Rohava Z, Balaji KN, Hoffner SE, Gaines H, Magalhaes I, Zumla A, Skrahina A, Maeurer MJ.** 2012. Pattern recognition and cellular immune responses to novel Mycobacterium tuberculosis-antigens in individuals from Belarus. BMC Infect. Dis. **12**:41. doi:10.1186/1471-2334-12-41.
7. **Bansal K, Elluru SR, Narayana Y, Chaturvedi R, Patil SA, Kaveri SV, Bayry J, Balaji KN.** 2010. PE_PGRS antigens of Mycobacterium tuberculosis induce maturation and activation of human dendritic cells. J. Immunol. **184**:3495–3504.
8. **Bansal K, Sinha AY, Ghorpade DS, Togarsimalemath SK, Patil SA, Kaveri SV, Balaji KN, Bayry J.** 2010. Src homology 3-interacting domain of Rv1917c of Mycobacterium tuberculosis induces selective maturation of human dendritic cells by regulating PI3K-MAPK-NF-kappaB signaling and drives Th2 immune responses. J. Biol. Chem. **285**:36511–36522.
9. **Bansal K, Trinath J, Chakravortty D, Patil SA, Balaji KN.** 2011. Pathogen-specific TLR2 protein activation programs macrophages to induce Wnt–beta-catenin signaling. J. Biol. Chem. **286**:37032–37044.
10. **Ghorpade DS, Kaveri SV, Bayry J, Balaji KN.** 2011. Cooperative regulation of NOTCH1 protein-phosphatidylinositol 3-kinase (PI3K) signaling by NOD1, NOD2, and TLR2 receptors renders enhanced refractoriness to transforming growth factor-beta (TGF-beta)- or cytotoxic T-lymphocyte antigen 4 (CTLA-4)-mediated impairment of human dendritic cell maturation. J. Biol. Chem. **286**:31347–31360.
11. **Kapoor N, Narayana Y, Patil SA, Balaji KN.** 2010. Nitric oxide is

involved in Mycobacterium bovis bacillus Calmette-Guerin-activated Jagged1 and Notch1 signaling. J. Immunol. **184**:3117–3126.
12. **Narayana Y, Balaji KN.** 2008. NOTCH1 up-regulation and signaling involved in Mycobacterium bovis BCG-induced SOCS3 expression in macrophages. J. Biol. Chem. **283**:12501–12511.
13. **Trinath J, Maddur MS, Kaveri SV, Balaji KN, Bayry J.** 2012. Mycobacterium tuberculosis promotes regulatory T-cell expansion via induction of programmed death-1 ligand 1 (PD-L1, CD274) on dendritic cells. J. Infect. Dis. **205**:694–696.
14. **Bansal K, Balaji KN.** 2011. Intracellular pathogen sensor NOD2 programs macrophages to trigger Notch1 activation. J. Biol. Chem. **286**:5823–5835.
15. **Bansal K, Kapoor N, Narayana Y, Puzo G, Gilleron M, Balaji KN.** 2009. PIM2 induced COX-2 and MMP-9 expression in macrophages requires PI3K and Notch1 signaling. PLoS One **4**:e4911. doi:10.1371/journal.pone.0004911.
16. **Bansal K, Narayana Y, Balaji KN.** 2009. Inhibition of TNF-alpha-induced cyclooxygenase-2 expression by Mycobacterium bovis BCG in human alveolar epithelial A549 cells. Scand. J. Immunol. **69**:11–19.
17. **Chaturvedi R, Bansal K, Narayana Y, Kapoor N, Sukumar N, Togarsimalemath SK, Chandra N, Mishra S, Ajitkumar P, Joshi B, Katoch VM, Patil SA, Balaji KN.** 2010. The multifunctional PE_PGRS11 protein from Mycobacterium tuberculosis plays a role in regulating resistance to oxidative stress. J. Biol. Chem. **285**:30389–30403.
18. **Narayana Y, Bansal K, Sinha AY, Kapoor N, Puzo G, Gilleron M, Balaji KN.** 2009. SOCS3 expression induced by PIM2 requires PKC and PI3K signaling. Mol. Immunol. **46**:2947–2954.
19. **A SK, Bansal Holla K, Verma-Kumar S, Sharma S, Balaji P, KN.** 2012. ESAT-6 induced COX-2 expression involves coordinated interplay between PI3K and MAPK signaling. Mol. Immunol. **49**:655–663.
20. **Huangfu D, Anderson KV.** 2006. Signaling from Smo to Ci/Gli: conservation and divergence of hedgehog pathways from Drosophila to vertebrates. Development **133**:3–14.
21. **Ingham PW, McMahon AP.** 2001. Hedgehog signaling in animal development: paradigms and principles. Genes Dev. **15**:3059–3087.
22. **Sasaki H, Nishizaki Y, Hui C, Nakafuku M, Kondoh H.** 1999. Regulation of Gli2 and Gli3 activities by an amino-terminal repression domain: implication of Gli2 and Gli3 as primary mediators of Shh signaling. Development **126**:3915–3924.
23. **Wen X, Lai CK, Evangelista M, Hongo JA, de Sauvage FJ, Scales SJ.** 2010. Kinetics of hedgehog-dependent full-length Gli3 accumulation in primary cilia and subsequent degradation. Mol. Cell. Biol. **30**:1910–1922.
24. **Di Marcotullio L, Ferretti E, Greco A, De Smaele E, Po A, Sico MA, Alimandi M, Giannini G, Maroder M, Screpanti I, Gulino A.** 2006. Numb is a suppressor of hedgehog signalling and targets Gli1 for Itch-dependent ubiquitination. Nat. Cell Biol. **8**:1415–1423.
25. **Fattorini L, Xiao Y, Ausiello CM, Urbani F, laSala A, Mattei M, Orefici G.** 1996. Late acquisition of hyporesponsiveness to lipopolysaccharide by Mycobacterium avium-infected human macrophages in producing tumor necrosis factor-alpha but not interleukin-1 beta and -6. J. Infect. Dis. **173**:1030–1034.
26. **Bailey JM, Mohr AM, Hollingsworth MA.** 2009. Sonic hedgehog paracrine signaling regulates metastasis and lymphangiogenesis in pancreatic cancer. Oncogene **28**:3513–3525.
27. **Sanchez P, Clement V, Ruiz i Altaba A.** 2005. Therapeutic targeting of the hedgehog-GLI pathway in prostate cancer. Cancer Res. **65**:2990–2992.
28. **Kaneko H, Yamada H, Mizuno S, Udagawa T, Kazumi Y, Sekikawa K, Sugawara I.** 1999. Role of tumor necrosis factor-alpha in Mycobacterium-induced granuloma formation in tumor necrosis factor-alpha-deficient mice. Lab. Invest. **79**:379–386.
29. **Liu M, Lee DF, Chen CT, Yen CJ, Li LY, Lee HJ, Chang CJ, Chang WC, Hsu JM, Kuo HP, Xia W, Wei Y, Chiu PC, Chou CK, Du Y, Dhar D, Karin M, Chen CH, Hung MC.** 2012. IKKalpha activation of NOTCH links tumorigenesis via FOXA2 suppression. Mol. Cell **45**:171–184.
30. **Nahid MA, Satoh M, Chan EK.** 2011. MicroRNA in TLR signaling and endotoxin tolerance. Cell. Mol. Immunol. **8**:388–403.
31. **Ghorpade DS, Leyland R, Kurowska-Stolarska M, Patil SA, Balaji KN.** 2012. MicroRNA-155 is required for Mycobacterium bovis BCG-mediated apoptosis of macrophages. Mol. Cell. Biol. **32**:2239–2253.
32. **Laird MH, Rhee SH, Perkins DJ, Medvedev AE, Piao W, Fenton MJ, Vogel SN.** 2009. TLR4/MyD88/PI3K interactions regulate TLR4 signaling. J. Leukoc. Biol. **85**:966–977.
33. **Rhee SH, Kim H, Moyer MP, Pothoulakis C.** 2006. Role of MyD88 in phosphatidylinositol 3-kinase activation by flagellin/Toll-like receptor 5 engagement in colonic epithelial cells. J. Biol. Chem. **281**:18560–18568.
34. **Tjiu JW, Chen JS, Shun CT, Lin SJ, Liao YH, Chu CY, Tsai TF, Chiu HC, Dai YS, Inoue H, Yang PC, Kuo ML, Jee SH.** 2009. Tumor-associated macrophage-induced invasion and angiogenesis of human basal cell carcinoma cells by cyclooxygenase-2 induction. J. Investig. Dermatol. **129**:1016–1025.
35. **Seto M, Ohta M, Asaoka Y, Ikenoue T, Tada M, Miyabayashi K, Mohri D, Tanaka Y, Ijichi H, Tateishi K, Kanai F, Kawabe T, Omata M.** 2009. Regulation of the hedgehog signaling by the mitogen-activated protein kinase cascade in gastric cancer. Mol. Carcinog. **48**:703–712.
36. **Kasperczyk H, Baumann B, Debatin KM, Fulda S.** 2009. Characterization of Sonic hedgehog as a novel NF-kappaB target gene that promotes NF-kappaB-mediated apoptosis resistance and tumor growth in vivo. FASEB J. **23**:21–33.
37. **Carmody RJ, Ruan Q, Palmer S, Hilliard B, Chen YH.** 2007. Negative regulation of Toll-like receptor signaling by NF-kappaB p50 ubiquitination blockade. Science **317**:675–678.
38. **Liew FY, Xu D, Brint EK, O'Neill LA.** 2005. Negative regulation of Toll-like receptor-mediated immune responses. Nat. Rev. Immunol. **5**:446–458.
39. **Negishi H, Ohba Y, Yanai H, Takaoka A, Honma K, Yui K, Matsuyama T, Taniguchi T, Honda K.** 2005. Negative regulation of Toll-like-receptor signaling by IRF-4. Proc. Natl. Acad. Sci. U. S. A. **102**:15989–15994.
40. **Wang J, Hu Y, Deng WW, Sun B.** 2009. Negative regulation of Toll-like receptor signaling pathway. Microbes Infect. **11**:321–327.
41. **O'Neill LA, Sheedy FJ, McCoy CE.** 2011. MicroRNAs: the fine-tuners of Toll-like receptor signalling. Nat. Rev. Immunol. **11**:163–175.
42. **O'Connell RM, Rao DS, Baltimore D.** 2012. microRNA regulation of inflammatory responses. Annu. Rev. Immunol. **30**:295–312.
43. **Arsenault RJ, Li Y, Maattanen P, Scruten E, Doig K, Potter A, Griebel P, Kusalik A, Napper S.** 31 October 2012. Altered Toll-like receptor 9 signaling in Mycobacterium avium subsp. paratuberculosis-infected bovine monocytes reveals potential therapeutic targets. Infect. Immun. [Epub ahead of print.] doi:10.1128/IAI.00785-12.
44. **Hirsch CS, Toossi Z, Vanham G, Johnson JL, Peters P, Okwera A, Mugerwa R, Mugyenyi P, Ellner JJ.** 1999. Apoptosis and T cell hyporesponsiveness in pulmonary tuberculosis. J. Infect. Dis. **179**:945–953.
45. **Nabeshima S, Nomoto M, Matsuzaki G, Kishihara K, Taniguchi H, Yoshida S, Nomoto K.** 1999. T-cell hyporesponsiveness induced by activated macrophages through nitric oxide production in mice infected with Mycobacterium tuberculosis. Infect. Immun. **67**:3221–3226.